Materials Advances

ROYAL SOCIETY OF CHEMISTRY

COMMUNICATION

View Article Online
View Journal | View Issue

Cite this: *Mater. Adv.*, 2025, **6**, 9380

Received 24th July 2025,
Accepted 13th November 2025

DOI: 10.1039/d5ma00803d

rsc.li/materials-advances

Redox active ZnO/2,5-dihydroxy terephthalic acid hybrid thin films prepared by one-step electrodeposition

Satoshi Chubachi, [a] Lauren Aheran, [b] Yuya Harada, [a] Tensho Nakamura, [ac] David Punihaole [b] and Tsukasa Yoshida *[a]

In this work we develop a simple, one-pot route to electrodeposit crystalline and porous ZnO/2,5-dihydroxy terephthalic acid (DHTPA) hybrid thin films. High loading of DHTPA was achieved up to half of the total film volume. The surface-bound DHTPA molecule undergoes a stable reversible redox reaction owing to the ion-exchanging capability of the porous ZnO, making this process a new promising approach to obtain active materials for electrochemical energy storage.

Hybridization of inorganic and organic materials is attractive since it often results in new concerted functionalities.[1–5] Chemistry between the constituents plays crucial roles in the success/failure of hybridization. We have observed various examples of electrochemically triggered self-assembly (ESA) of inorganic compound thin films hybridized with organic molecules, typically aromatic organic dyes.[6–11] For example, organic dyes bearing anionic acidic anchoring groups, such as eosin Y (EY^{2-}), yield ZnO/dye hybrid thin films when they are added to the bath for cathodic electrodeposition of ZnO,[7,8,12,13] whereas those with cationic functionalities such as dimethylaminostylbazolium (DAS^{+}) selectively hybridize with CuSCN during its electrodeposition.[5,10,11]

Highly porous, crystalline, sponge-like ZnO as described above serves as a good photoelectrode when suitable photosensitizer dyes are adsorbed.[8,14] In such hybrid materials, photoexcited states of the dye molecules are able to inject electrons to the conduction band of ZnO.[15,16] When redox-active organic molecules are bound, the hybrid materials are expected to undergo reversible redox reactions. The porous ZnO can potentially act as a highly conductive scaffold with a high surface area to stabilize the attachment of the redox molecule, while providing pathways for ionic transport.

Here, we hybridize 2,5-dihydroxy terephthalic acid (DHTPA) with ZnO by one-step electrodeposition. DHTPA is a variant of terephthalic acid (TPA, benzene-1,4-dicarboxylic acid), but can undergo a reversible redox reaction (Scheme 1) just like a hydroquinone (HQ)/benzoquinone (BQ) pair. We previously demonstrated that we could obtain Zn-TPA metal–organic frameworks (MOFs) by a microwave-assisted hydrothermal reaction,[17] as well as electrodeposition[18] from mixtures of Zn^{2+} and TPA. Based on these previous findings, we therefore anticipate strong coordination of two carboxylates at 1,4 positions of DHTPA to ZnO surface during the electrodeposition.

Our initial results in this report indicate that these Zn/DHTPA hybrid thin films have reversible redox capabilities. We examine the impact of gradual addition of DHTPA in terms of hybrid composition, crystallinity and morphology. We also present results on the redox properties of ZnO/DHTPA hybrid thin films and discuss their implication as novel active materials in electrochemical energy storages.

Chronoamperograms during the electrodeposition are shown in Fig. 1(a). Following the initial peak associated with the nucleation of ZnO,[19] a steady-state current of *ca.* 1.3 mA cm^{-2} is observed in the absence of DHTPA, which is close to the diffusion limit of the $2e^{-}$ oxygen reduction reaction (ORR) at ω = 500 rpm. Nakamura *et al.*[20] has found that the full $4e^{-}$ ORR down to OH^{-} is strongly suppressed in the presence of Zn^{2+} ions in solution, so that the formation of ZnO is predominantly

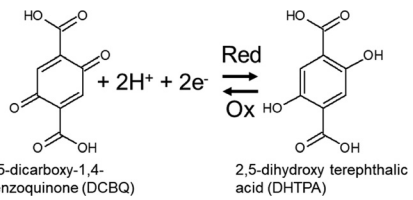

Scheme 1 Redox reaction of DHTPA and DCBQ.

[a] *Graduate School of Organic Materials Science, Yamagata University, 4-3-16 Jonan, Yonezawa, Yamagata 992-8510, Japan*
[b] *Department of Chemistry, University of Vermont, 82 University Place, Burlington, VT 05405, USA*
[c] *Graduate school of Engineering, Gifu University, 1-1 Yanagido, Gifu City 501-1193, Japan*

associated with co-production of H_2O_2. Upon addition of DHTPA, the initial current peak is delayed and obscured, while the steady-state current is slightly decreased, due to hindrance of the ORR and ZnO growth by the surface attachment of DHTPA. When DHTPA is added at 500 μM, a drastic change occurs in which a significant decrease of current over the period is observed, although it does not reach zero over the course of the electrolysis.

The X-ray diffraction (XRD) patterns of the product thin films (Fig. 1(b)) show crystallization of ZnO. This conclusion based on the three major peaks observed at 2θ = 31.7°, 34.4° and 36.2° for the electrodeposited film products produced both in the absence and presence of DHTPA up to a concentration of 400 μM. These peaks can be ascribed to diffraction of the (100), (002) and (101) planes, respectively, of ZnO. At 500 μM, however, these peaks almost disappear. The absence of conductive ZnO can account for the gradual decrease of current during the electrodeposition. Careful examination of the XRD patterns also reveals a decreasing trend of the preferential orientation of crystallites upon increasing DHTPA. While pure ZnO is strongly oriented with its *c*-axis perpendicular to the substrate as indicated by its prominent (002) diffraction peak, those electrodeposited with DHTPA are less oriented, showing smaller differences of the peak heights, decreased intensity and slight broadening of the three diffraction peaks.

Formation of ZnO/DHTPA hybrid thin films was additionally confirmed by spectroscopic analysis (Fig. 2) of their chemical compositions. Although partial formation of amorphous $Zn(OH)_2$ may have occurred during ZnO electrodeposition, the calculations of faradaic efficiency and volume ratio assumed that all the Zn^{2+} detected by ICP-MS were used to form ZnO (see Note S1 in the SI for details). The amount of charge and electrodeposited ZnO decreases, despite the faradaic efficiency remaining constant at around 90%, as the concentration of DHTPA increases in the bath. In contrast, the amount of DHTPA loaded into the film increases with concentration, although not proportionally at concentrations above 400 μM. This suggests that the loading is not limited by transportation of DHTPA, but by the stability of the surface complex between ZnO and DHTPA.

The DHTPA/ZnO volume ratio, estimated by assuming the density of solid DHTPA to be 1.42 $cm^3\ g^{-1}$, can let us envision how the two components hybridize. It exceeds 0.9 at DHTPA = 500 μM, so that almost half of the film volume is occupied by that of DHTPA. The loading of DHTPA at such a high amount can hinder the formation of ZnO crystals and thus can cause its absence under this condition.

Although the film thickness was in the range of 0.7–0.8 μm, irrespective of the presence and absence of DHTPA, co-precipitation of DHTPA did result in a significant change of surface morphology, as seen in the scanning electron microscope (SEM) images (Fig. 3). The pure ZnO thin film exhibits hexagonally shaped flat facet of (002), as expected from its strong crystallographic orientation. Evolution of the own shape

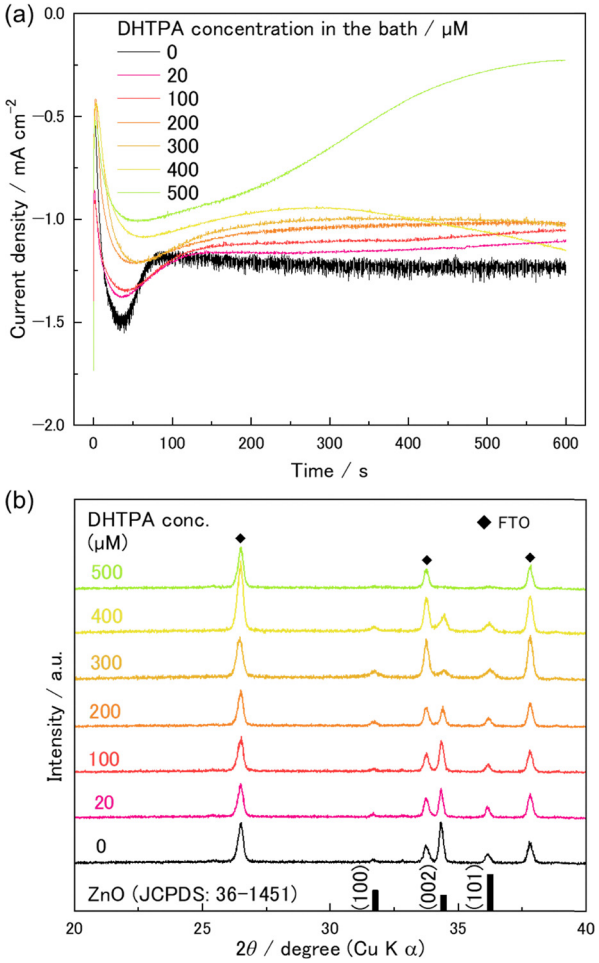

Fig. 1 (a) Chronoamperograms during potentiostatic electrolysis at −1.00 V *vs.* Ag/AgCl in O_2-saturated aqueous solutions containing 5 mM $ZnCl_2$, 50 mM KCl and 0, 20, 100, 200, 300, 400 and 500 μM DHTPA. Solutions were adjusted to pH 6.00 with HCl/KOH. (b) XRD patterns of the electrodeposited thin film products in comparison with the JCPDS pattern of ZnO (36-1451).

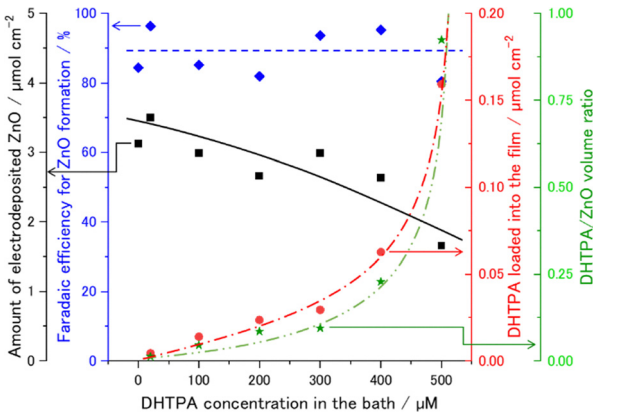

Fig. 2 Change of ZnO electrodeposition and loading of DHTPA molecule into the hybrid thin films as a function of DHTPA concentration in the bath; amount of electrodeposited ZnO determined from ICP-MS analysis (■), faradaic efficiency for ZnO formation (◆), amount of DHTPA loaded into the film as analyzed by UV-vis absorption (●) and the estimated DHTPA/ZnO volume ratio of the hybrid thin films (★).

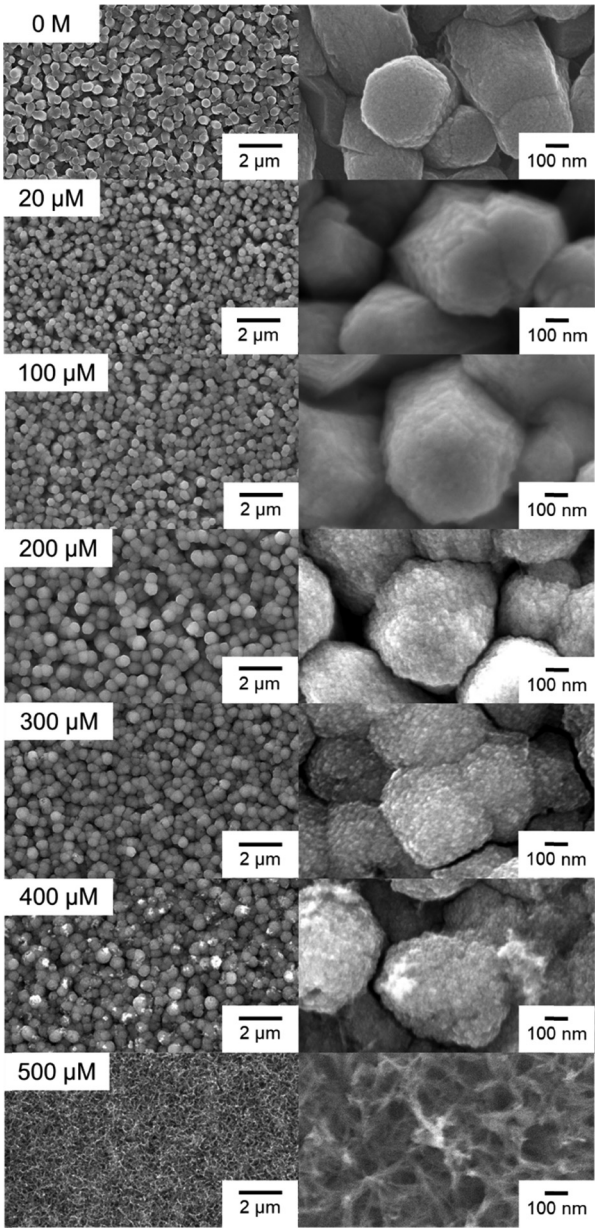

Fig. 3 SEM images of the films electrodeposited at each concentration.

of ZnO, despite its diffusion-limited growth, suggests a strong reversibility of the precipitation, namely, dissolution/re-crystallization reactions to shape the particles. On increasing addition of DHTPA, the particles become round and eventually change to a reticulated, ill-shaped deposit at 500 μM. The hexagonal shape of the particles is still preserved at concentrations up to 100 μM, but they become spherical and exhibits tiny nanostructured features upon further addition of DHTPA. Such changes are characteristic of hybridization of ZnO with organic molecules, as understood from the studies for the ESA with EY^{2-}.[14] While these nano-morphological features are caused by the loading of DHTPA, the hemispherical top of the deposits suggests irreversible precipitation that reflects the mass transport, which is naturally anisotropic. As the DHTPA molecule strongly binds, ZnO is also stabilized in return, so that reconstruction by a dissolution/re-crystallization sequence operates less. As we have learned from the XRD, crystal growth of ZnO is not completely hindered by DHTPA as it is segregated and not resulting in a formation of a MOF with a definitive composition and distinctive crystal structure, although MOF74 in a Zn_2(DHTPA) composition is indeed known.[21]

FTIR measurements were performed on films electrodeposited at 0, 200, and 500 μM DHTPA to discern the molecular nature of the interactions between DHTPA and ZnO in the hybrid films (see SI for details). The FTIR spectrum of DHTPA powder showed the characteristic COOH and C–O stretching vibrations 1650 and 1200 cm^{-1}, respectively (Table S1).[22] In contrast, the spectrum of the film electrodeposited at 0 M exhibited no ZnO-related absorption bands, and only minor features attributable to atmospheric CO_2 at 2350 cm^{-1}. For the films electrodeposited at 200 and 500 μM DHTPA, new bands appeared at *ca.* 1550 and 1400 cm^{-1}.[23]

To interpret these bands, we performed density functional theory (DFT) calculations on DPHTA compounds bound to Zn atoms in two different coordination geometries (Fig. 5). The calculations for all the models that we considered in Fig. 5 indicate that the 1541 and 1414 cm^{-1} bands observed in the FTIR spectra (Fig. 4) derive from vibrational modes that contain significant contributions from carboxylate stretching, ring stretching, and CH and OH deformations to their eigenvector compositions (see Table S2 and Fig. S3). Our DFT calculations suggest that the vibrational frequencies of the surface-binding models seen in Fig. 5 qualitatively agree with the experimental FTIR spectra (see Table S2 and Fig. S2). For the chelated model (Fig. 5a) the calculated carboxylate modes are predicted to occur at 1527, 1483 cm^{-1}, 1403, and 1357 cm^{-1} (Table S2). For the monodentate bridge model (Fig. 5b) the calculated carboxylate modes are predicted to occur at 1526, 1496 cm^{-1},

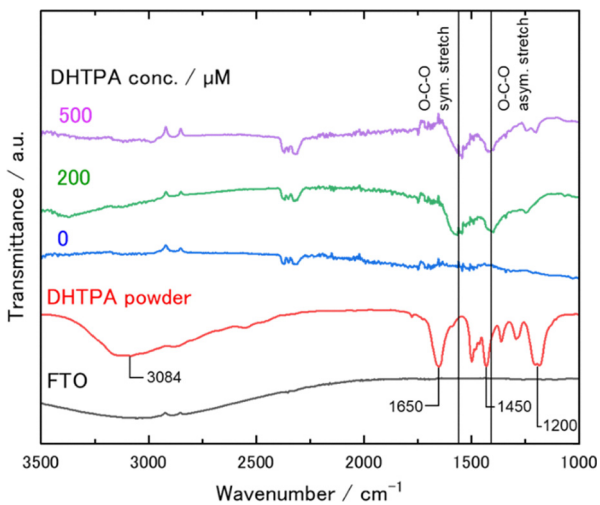

Fig. 4 ATR-FTIR spectra of FTO substrate and films electrodeposited in 50 mM KCl, 5 mM $ZnCl_2$, 0, 200 and 500 μM DHTPA aqueous solution saturated with O_2 at −1.00 V *vs.* Ag/AgCl for 20 min. KBr-FTIR spectrum of DHTPA powder.

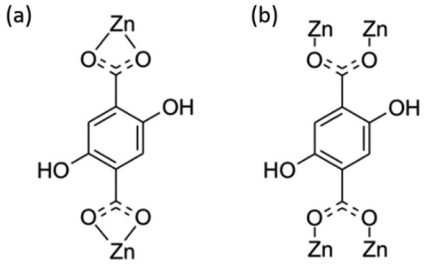

Fig. 5 Illustration of possible carboxylate coordination geometries of DHTPA at the ZnO interface: (a) chelating, and (b) monodentate bridging.

1407 and 1331 cm^{-1} (Table S2). These predicted modes correspond to the assigned FTIR bands at 1541 and 1414 cm^{-1} for the 500 μM DHTPA film and the bands at 1564 and 1398 cm^{-1} for 200 μM DHTPA. Thus, our analysis indicates that the carboxylic acid moieties of DHTPA deprotonate in the hybrid films and coordinate to ZnO through these two potentials coordination geometries.

The colorless and typically translucent ZnO/DHTPA hybrid thin films are then evaluated for their redox properties. Cyclic voltammograms (CVs) are compared for films with different degree of DHTPA loading (Fig. 6(a)). While pure ZnO does not show any redox signals, those electrodeposited with increasing concentration of DHTPA exhibit prominent reversible redox peaks centred at around −0.53 V, which arise from the redox of the loaded DHTPA. For the sample electrodeposited with 400 μM DHTPA, however, a new cathodic peak appears at around −0.25 V. The redox behavior then further changes to a completely different one at 500 μM, which shows a broad oxidation feature in the CV above −0.2 V, countered to a sharp cathodic peak at around −0.4 V. Although these characters of the 500 μM sample should also originate from DHTPA loaded into the film with a different chemical environment from the others, they were not stable and changed to CVs similar to those of the samples grown below 300 μM DHTPA upon repetition of potential cycling, implying its irreversible chemical change.

The film with 200 μM DHTPA was further analysed. Fig. 6(b) shows the CVs at different scan rates between 5 and 100 mV s^{-1}. Peak positions do not change, and their magnitude is proportional to the scan rate (Fig. 6(c)), indicating no suppression of the redox reactions by diffusion.[24,25] Such fast redox reactions are typically expected for surface-bound redox species. Porous structures of sponge-like ZnO crystals are beneficial for fast transport of electron and ions in solar cell applications.[26,27] Although the absolute capacity is currently limited by the small film thickness, this electrodeposited ZnO/DHTPA hybrid thin film can be an interesting candidate to be studied further for energy storage in batteries or redox capacitors, especially due to its fast redox response.

Finally, the pH dependence of the redox reaction was studied (Fig. 6(d)). The redox potential ($E_{1/2}$) shifted in a complex manner (Fig. 5(e)): −68 mV pH^{-1} for pH < 5, almost constant around −0.53 V for 5 < pH < 9, and becomes dependent again as −54 mV pH^{-1} for 9 < pH. The slopes

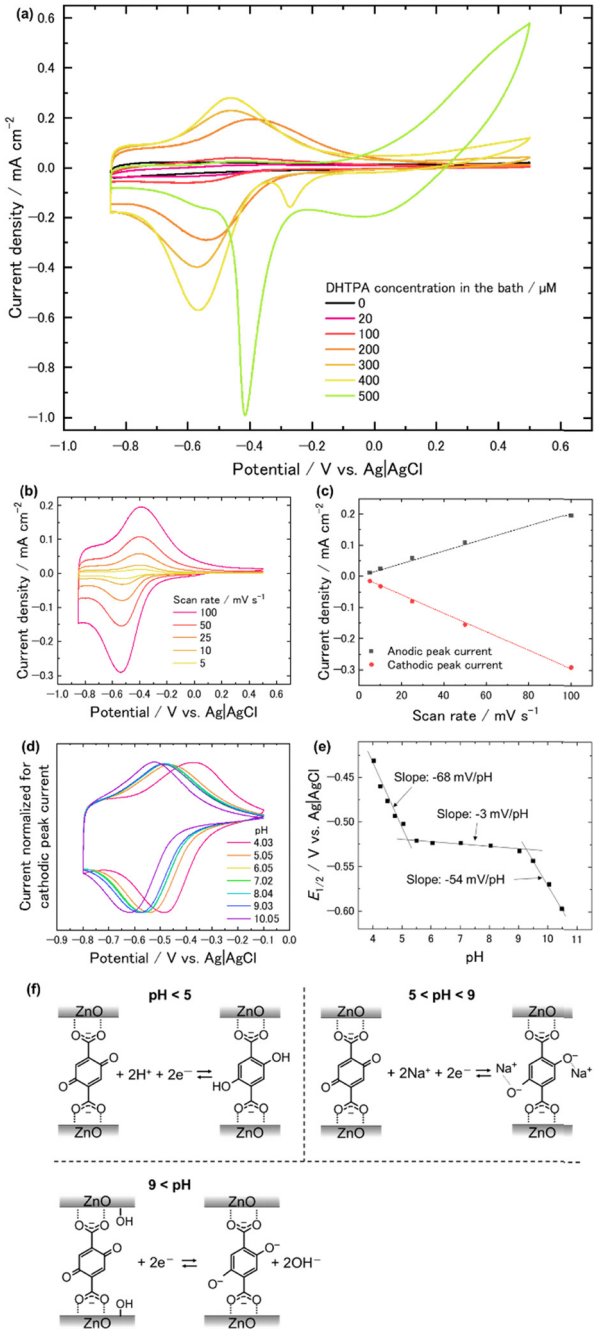

Fig. 6 (a) Cyclic voltammograms (CVs) measured at the ZnO/DHTPA hybrid thin film electrodes for variation of DHTPA concentration in the electrodeposition bath, with a fixed scan rate v = 100 mV s^{-1} in a 1.0 M Na_2SO_4 aqueous solution (pH 7.0), (b) CVs on variation of v at that grown with 200 μM DHTPA, (c) peak current *vs.* v plots drawn from (b), (d) CVs at the same ZnO/DHTPA electrode on variation of the electrolyte pH between 4 and 10 as adjusted by adding small amount of H_2SO_4 or NaOH, (e) $E_{1/2}$ *vs.* pH plot drawn from (d), and (f) schematic illustration of the plausible redox reactions in different pH ranges.

close to 59 mV/pH suggest the same number of protons or hydroxides as electrons to be coupled for the redox of DHTPA. It is straightforward to consider two-electron and two-proton-coupled HQ/BQ type of redox in the acidic region.[25,28] In the pH independent neutral range, the charge compensation

should be achieved by exchange of the supporting electrolyte, probably that of Na^+. Then, the steep pH dependent shift in the basic region is most likely achieved by hydroxylation of ZnO matrix in proximity of DHTPA. The overall electrochemical stoichiometry in each pH regime can therefore be illustrated as Fig. 6(f).

Conclusions

As expected from the chemical structure of DHTPA, hybridization of DHTPA with ZnO has been successfully achieved. Thus, the ZnO/DHTPA hybrid thin films that we prepared exhibited fast reversible redox originating from DHTPA. The porous ZnO with a high surface area not only provides pathways for ionic transport, acts as scaffolds for stable attachment of DHTPA, but also supports the redox by exchanging hydroxide ions. Although the exact nanostructure, redox capacity and stability are yet to be scrutinized, the electrochemically self-assembled ZnO/DHTPA hybrid thin film can be nominated as a unique and interesting candidate of active materials in electrochemical energy storage devices.

Author contributions

Satoshi Chubachi and Tsukasa Yoshida conceived the idea, and Satoshi Chubachi performed experiments. Yuya Harada and Tensho Nakamura provided helpful suggestions. Satoshi Chubachi and Tsukasa Yoshida wrote the manuscript. Lauren Aheran and David Punihaole performed DFT calculations and helped interpret FTIR spectra. Lauren Aheran and David Punihaole helped edit the manuscript. All authors discussed the results and commented on the manuscript.

Conflicts of interest

There are no conflicts to declare.

Data availability

The data supporting this article have been included as part of the supplementary information (SI). Supplementary information: the experimental method and methods to determine the values plotted in Fig. 2 have been included as part of the SI. See DOI: **https://doi.org/10.1039/d5ma00803d**.

Acknowledgements

This material is based upon work jointly supported by JSPS (JPJSJRP20221201) and NSF (OISE-2230706) in 2023–2025 Partnership for International Research and Education (PIRE), ''US–Japan Partnership in Excitonic Soft Materials for Clean Energy''. This study was also supported by: Grant-in-Aid for Scientific Research (Kakenhi, 24K01596) from Japan Society for Promotion of Science (JSPS); the establishment of University fellowships towards the creation of science technology innovation of JST (Grant Number JPMJFS2104); Experimental equipment sharing system, Yamagata University X-ray diffractometer (Rigaku, SmartLab), scanning electron microscope (SEM, JEOL, JSM-IT800) and inductively coupled plasma mass spectroscopy (ICP-MS, Perkin-Elmer, ELAN DRC II).

Notes and references

1 C. Sanchez, B. Julián, P. Belleville and M. Popall, *J. Mater. Chem.*, 2005, **15**, 3559–3592.
2 J. Gong, K. Sumathy, Q. Qiao and Z. Zhou, *Renewable Sustainable Energy Rev.*, 2017, **68**, 234–246.
3 S. Wang, Y. Kang, L. Wang, H. Zhang, Y. Wang and Y. Wang, *Sens. Actuators, B*, 2013, **182**, 467–481.
4 H. Yang, K. Dai, J. Zhang and G. Dawson, *Chin. J. Catal.*, 2022, **43**, 2111–2140.
5 K. Uda, Y. Tsuda, S. Okada, R. Yamakado, L. Sun, Y. Suzuri, M. S. White, M. Furis, P. Stadler, O. Dimitriev and T. Yoshida, *ACS Omega*, 2019, **4**, 4056–4062.
6 T. Yoshida, J. Zhang, D. Komatsu, S. Sawatani, H. Minoura, T. Pauporté, D. Lincot, T. Oekermann, D. Schlettwein, H. Tada, D. Wöhrle, K. Funabiki, M. Matsui, H. Miura and H. Yanagi, *Adv. Funct. Mater.*, 2008, **19**, 17–43.
7 S. Karuppuchamy, T. Yoshida, T. Sugiura and H. Minoura, *Thin Solid Films*, 2001, **397**, 63–69.
8 T. Yoshida, J. Yoshimura, M. Matsui, T. Sugiura and H. Minoura, *Trans. Mater. Res. Soc. Jpn.*, 1999, **24**, 497–500.
9 T. Yoshida and H. Minoura, *Adv. Mater.*, 2000, **12**, 1219–1222.
10 Y. Tsuda, H. Sun, L. Sun, S. Okada, A. Masuhara, P. Stadler, N. S. Sariciftci, M. S. White and T. Yoshida, *Monatsh. Chem.*, 2017, **148**, 845–854.
11 Y. Tsuda, K. Uda, M. Chiba, H. Sun, L. Sun, M. S. White, A. Masuhara and T. Yoshida, *Microsyst. Technol.*, 2017, **24**, 715–723.
12 T. Pauporte, T. Yoshida, R. Cortes, M. Froment and D. Lincot, *J. Phys. Chem. B*, 2003, **107**, 10077–10082.
13 K. Okabe, T. Yoshida, T. Sugiura and H. Minoura, *Trans. Mater. Res. Soc. Jpn.*, 2001, **26**, 523–526.
14 H. Minoura and T. Yoshida, *Electrochemistry*, 2008, **76**, 109–117.
15 I. Minda, E. Ahmed, V. Sleziona, C. Richter, M. Beu, J. Falgenhauer, H. Miura, D. Schlettwein and H. Schwoerer, *Phys. Chem. Chem. Phys.*, 2016, **18**, 8938–8944.
16 J. A. Anta, E. Guillén and R. Tena-Zaera, *J. Phys. Chem. C*, 2012, **116**, 11413–11425.
17 Y. Hirai, K. Furukawa, H. Sun, Y. Matsushima, K. Shito, A. Masuhara, R. Ono, Y. Shimbori, H. Shiroishi, M. S. White and T. Yoshida, *Microsyst. Technol.*, 2017, **24**, 699–708.
18 T. Nakamura, S. Ueda, K. Uda, Y. Tsuda, Y. Hirai, H. Sun and T. Yoshida, *ECS Trans.*, 2019, **88**, 343–350.
19 S. Peulon and D. Lincot, *J. Electrochem. Soc.*, 1998, **145**, 864–874.
20 T. Nakamura, K. Ikeda, H. Morinaga and T. Yoshida, *Electrochemistry*, 2024, **92**, 107001.
21 N. L. Rosi, J. Kim, M. Eddaoudi, B. Chen, M. O'Keeffe and O. M. Yaghi, *J. Am. Chem. Soc.*, 2005, **127**, 1504–1518.

22 M. J.-M. Takač and D. V. Topić, *Acta Pharm.*, 2004, **54**, 177–191.
23 V. Zeleňák, Z. Vargová and K. Györyová, *Spectrochim. Acta, Part A*, 2007, **66**, 262–272.
24 A. J. Bard, L. R. Faulkner and H. S. White, *Electrochemical Methods: Fundamentals and Applications*, Wiley, Hoboken, 3rd edn, 2022.
25 C. M. Hanna, A. Luu and J. Y. Yang, *ACS Appl. Energy Mater.*, 2019, **2**, 59–65.
26 T. Oekermann, T. Yoshida, H. Minoura, K. G. U. Wijayantha and L. M. Peter, *J. Phys. Chem. B*, 2004, **108**, 8364–8370.
27 T. Oekermann, T. Yoshida, C. Boeckler, J. Caro and H. Minoura, *J. Phys. Chem. B*, 2005, **109**, 12560–12566.
28 C. Costentin, *Chem. Rev.*, 2008, **108**, 2145–2179.